New corrosion resistant multicomponent alloys for use in fuel cells

Project Report

Summary of the results

A total amount of 497 kSEK was granted by ÅForsk to Uppsala University to carry out a project investigating inexpensive multicomponent corrosion resistant coatings to be used in fuel cells with a possibility of expanding their use in any other industrial application, where conventional stainless-steels are used. Access to such coatings can have a large impact on the development of fossil-free sustainable vehicles, decreasing the emission of pollutant gases [1-3]. The composition of the multicomponent alloy CrMnFeCoNi [4] was used as a starting material, because its composition is an extension of stainless steel and is known for its excellent mechanical properties, and formability [5]. Preliminary results [6] had showed that the addition of carbon in the CrMnFeCoNi multicomponent coatings could improve their corrosion resistance. The corrosion resistance of near equimolar CoCrFeMnNi magnetron-sputtered coatings produced in the Inorganic department of the Uppsala University embedded with different carbon concentrations (i.e. 0 , 7 at.% and 11 at.% C) was estimated in acidic environments, such as 0.05 M H_2SO_4 and 0.05 M HCl, because in terms of applications the low pH conditions are preferable to be tested (i.e. coating production for PEM fuel cells applications). Further corrosion studies performed within this project to explore the role of carbon and the reasons for offering a higher corrosion resistance in the coatings. The evaluation of the corrosion resistance of the coatings was done by use of electrochemical means including: open circuit potential measurements (OCP), electrochemical impedance spectroscopy (EIS), polarization curves, and microscopy (SEM/EDS) and spectroscopy (XPS) means. The selection of HCl electrolyte was due to the fact that Cl^- ions result in pitting corrosion phenomena on stainless steel compositions. The electrochemical results showed that no significant differences were observed for the films in the passive region when carrying out the experiments in 0.05 M H_2SO_4 and 0.05 M HCl, respectively, but the concentration of carbon and the choice of electrolyte, however, affected the current in the transpassive region, at potentials above 0.85 V vs. Ag/AgCl (3M NaCl). The carbon-containing films were more corrosion resistant

in 0.05 M HCl than in 0.05 M H_2SO_4, in the transpassive region, due to a lower carbon oxidation rate, which facilitated the formation of a Mn-rich oxide layer. This is a very important finding in terms of corrosion, because a stainless-steel composition is not corrosion resistant at high potentials due to further oxidation of Cr, while in the presence of Cl^- ions its corrosion resistance suffers from pitting corrosion.

Introduction

Stainless steel, which is one of the most common used material in industry, which is also used to manufacture parts of fuel cells such as bipolar plates (BPs) [7]. In terms of the corrosion resistance, a stainless steel is sensitive to corrosion as it only contains one passive element (i.e. Cr) and the formed Cr_2O_3 passive layer, but is not stable above 0.8 V vs. Ag/AgCl in acidic electrolytes [8,9]. This can be a problem in terms of applications. For example, a stainless steel made cathode BPs in a PEM fuel shows a significantly decreased corrosion resistance due to pitting corrosion, in presence of of F^- (or Cl^-) ions, which are typically are present in a cell. The equimolar CrFeNiCoMn high entropy alloy was used as a testing material in this study, because its composition is an extension of the stainless-steel composition, and shows excellent mechanical properties. Preliminary results [6] had showed that the addition of carbon could results in amorphous coatings with an improved corrosion resistance in H_2SO_4, while lower corrosion resistance in the transpassive region was observed in 0.05 M HCl. Electrochemical experiments, including polarization curves and impedance spectroscopy (EIS) were performed in this project to further understand the role of carbon in different acidic environments. The electrochemical results were further analysed in combination of spectroscopy and microscopy techniques.

Experimental methods

Sample preparation: CoCrFeMnNi thin films, with and without carbon, were deposited by dc magnetron co-sputtering on Si substrates with a 1.5 μm thick amorphous oxide, grown by dry oxidation.

Corrosion studies: The samples were tested electrochemically using different electrolytes, e.g. H_2SO_4 and HCl. Each sample was used as the working electrode in a three-electrode electrochemical cell connected to a potentiostat, using a Ag/AgCl (3 M NaCl) reference electrode

and a Pt wire as the counter electrode. Polarization curves and EIS data were recorded to evaluate the electrochemical performances of the coatings.

Characterization of the samples: X-rays photoelectron spectroscopy (XPS) and scanning electron microscopy (SEM-EDS) were used to study the morphology and composition of the coatings before and after corrosion. The SEM images of the films were checked with a Zeiss Merlin scanning electron microscopy (SEM) instrument, while the concentration of the metallic elements was recorded by energy dispersive X-ray analysis (EDX) analyzed using the AZtec (INCA energy) software. X-rays Photoelectron spectroscopy (XPS) investigations were performed with a PHI Quantera II scanning XPS microprobe using monochromatic Al Kα radiation ($h\nu$ = 1486.7 eV).

Results and discussion:

The most important electrochemical, spectroscopy and imaging experimental findings followed by a short discussion are summarized in this report.

Surface morphology: The top-view SEM images show that the carbon free film exhibits a complex morphology on its surface with several features composed of smaller (around 15 nm) and larger diameters features (about 50 nm) (Fig.1a). The addition of carbon (i.e. about 7 at.% C and about 11 at.% C) results in dense, smooth and free from grain boundaries films (Fig. 1b and c). The carbon concentration was estimated by an XPS depth profile. The thickness was estimated from the cross-section SEM images and found to be around 650nm for all films. The cross-section SEM images for the carbon free sample show a nanocolumnar structure (Fig. 1d), while a vein pattern is observed for the carbon contained samples due to plastic deformation inside the shear bands (Fig.1 e and f). An EDS mapping (Fig. 2) on both carbon free and carbon containing samples, showed no elemental segregation in the films.

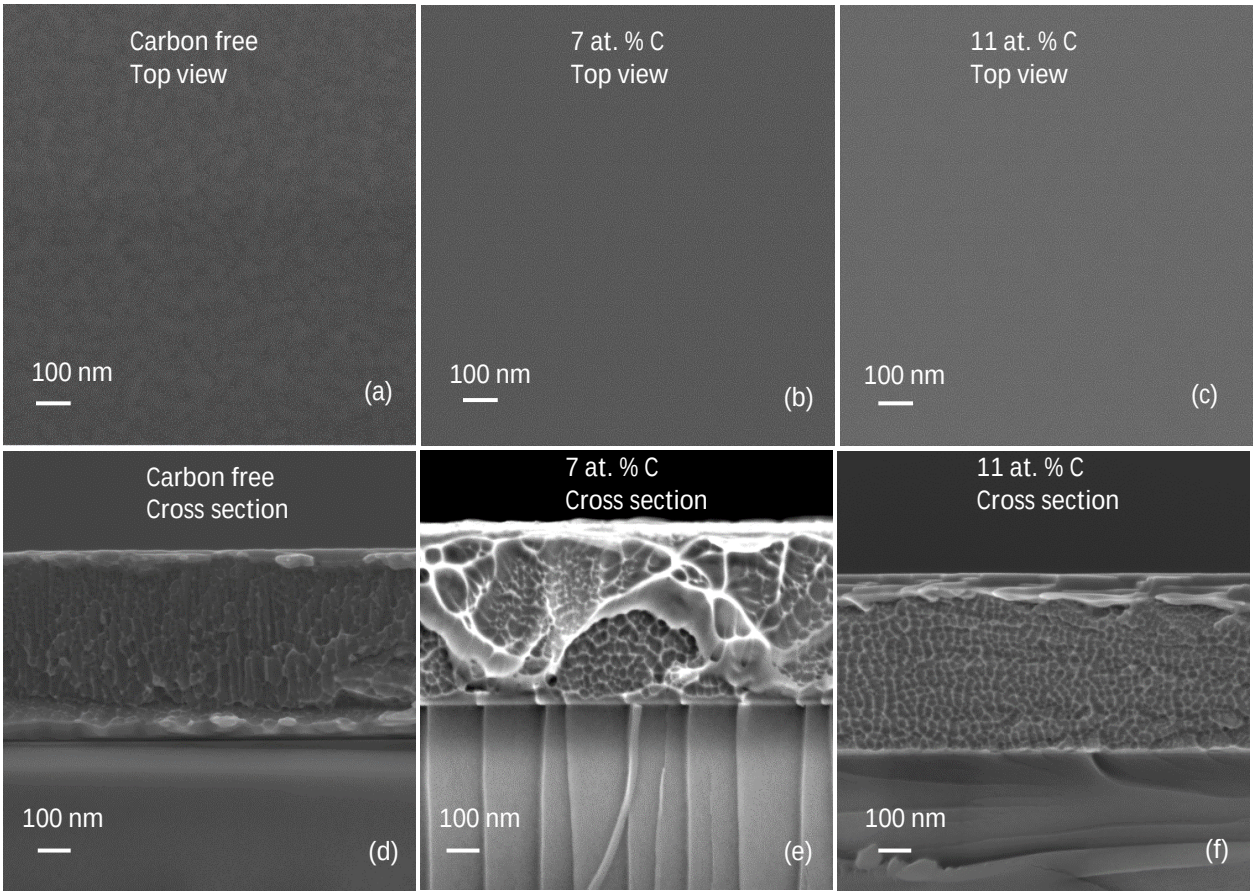

Figure 1: Top view (first row) and cross-section (second row) SEM images for the carbon free and carbon contained CoCrFeMnNi coatings

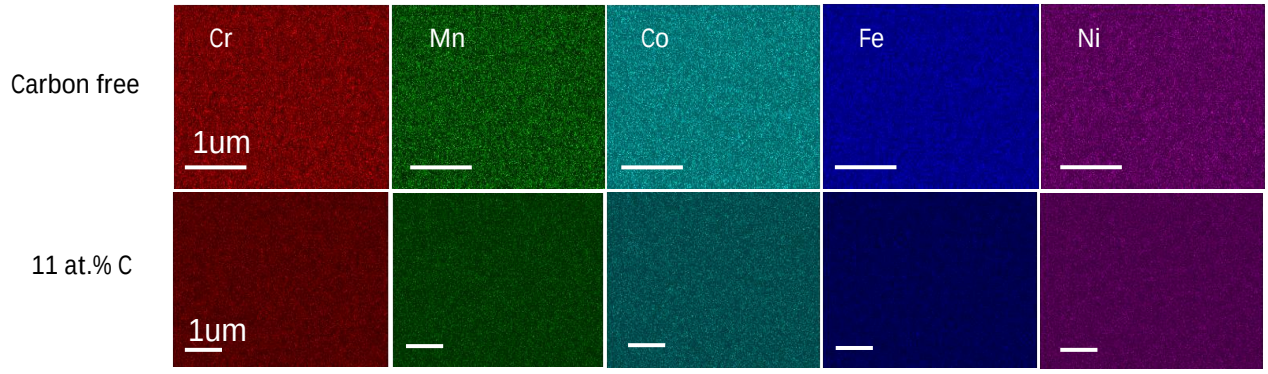

Figure 2: EDS mapping for a carbon free and a ~11 at.% C sample. The results showed that there is no elemental segregation in the films.

The average elemental compositions estimated from five different sample pieces from each group (i.e. carbon free, ~7 at.% and ~11% at. carbon), produced with the same sputter parameters are given in Table 1. The ratio of the five metals was close to equimolar ratio for the carbon-free sample. The concentration of Mn for the carbon contained films was decreasing with increasing carbon content. This was probably related to the sputter conditions. For a higher carbon content in the coatings, an increased graphite target power was needed during the deposition, which probably resulted in a changed plasma density affecting the most volatile Mn content (for unknown reasons).

Table 1: SEM/EDS composition for thin films

Sample	Cr	Mn	Fe	Co	Ni
Carbon free film	19.0 ±0.1	19.1 ±0.1	20.8±0.1	19.9 ±0.1	21.1 ±0.1
~ 7%C film	20.4 ±0.6	14.2 ±1.6	22.2 ±1.0	21.0 ±0.6	22.0 ±0.6
~ 11%C film	20.7 ±0.2	11.5 ±1.3	22.3 ±0.5	21.4 ±0.2	21.8 ±0.5

Electrochemical results

The corrosion resistance of the films was estimated in acidic environments, such as 0.05 M H_2SO_4 and 0.05 M HCl. The electrochemical results including OCP, EIS and polarization curves are given and discussed below.

- Experiments in 0.05 M H_2SO_4

Prior to polarization curves the films were left under OCP conditions for 45 minutes, reaching values about 0.20V, 0.22V and 0.26V vs. Ag/AgCl for the samples with 0, 7 and 11 at.% C respectively (Fig. 3a). During the OCP experiments the potential is a mixed potential involving a passive layer that is already present prior to the experiment. More noble OCP values are linked to more corrosion resistant oxides. Electrochemical Impedance spectroscopy (EIS) was performed under OCP, including Nyquist and Bode plots (Fig 3c and 3d). In the Nyquist diagram, the plots tend to be as a straight line close to the imaginary axis, indicating a ''capacitive'' behaviour and

high corrosion resistant for the coatings under OCP conditions. In the phase Bode plot, the phase angle is between 83.6° to 84.7° degrees at the lowest frequency value (100 mHz). For a phase angle equal to 90°, an ideal capacitive behaviour is achieved. After OCP, the potential was scanned from –0.7 to 1.4 V vs. Ag/AgCl in H_2SO_4 and the Fig. 2b shows the polarization curves for the carbon-free and the carbon contained films. The E_{corr} is slightly shifted to more noble values for the carbon contained films i.e. -0.34V vs Ag/AgCl for the carbon-free sample, -0.32V and -0.30V vs Ag/AgCl for the ~7 at.% C and ~11at.% C respectively. The j_{corr} values were estimated by using Tafel lines extrapolation and found about 9.6×10^{-6} A/cm^2 for the carbon-free film, 7.3×10^{-6} A/cm^2 and 2.6×10^{-6} A/cm^2 for the ~7 at.% C and ~11 at.% C respectively. A nobler E_{corr} value along with a lower i_{corr} value indicates that the carbon contained samples are more corrosion resistant around the E_{corr}. Significant differences in the polarization curves were observed in the transpassive region, between the carbon free and the carbon containing samples. The transpassive region started at about 0.85 V vs Ag/AgCl for all samples, which is mainly attributed to further oxidation of Cr_2O_3 to soluble Cr(VI). For the carbon free sample, a significant current decrease was observed above 1.2 V vs Ag/AgCl, while the current density increases reaching about 0.01A/cm^2 at 1.4 V vs Ag/AgCl for the carbon containing samples. After the polarization curves microscopy and XPS measurements were performed to further analyze the samples. The XPS results are given below in a separate paragraph of this report.

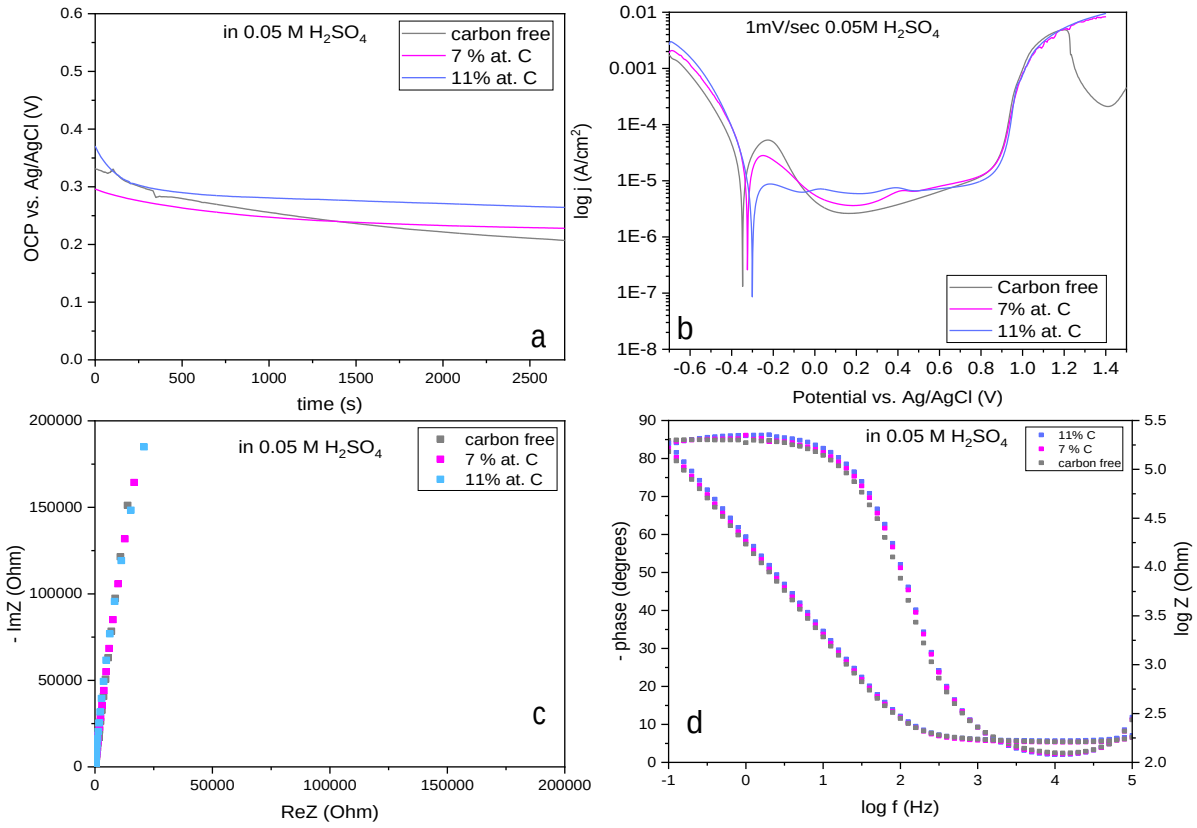

Figure 3: Electrochemical experiments in 0.05 M H_2SO_4: (a) Open circuit potential (OCP) vs. time plot, (b) polarization curves from -0.7 V to 1.5 V vs Ag/AgCl with a scan rate of 1 mV/s (c) Nyquist and (d) Bode plots obtained after 45 minutes at the OCP.

- Experiments in 0.05 M HCl

Prior to polarization curves in 0.05 M HCl, the films were left under OCP conditions, reaching values about 0.08V, 0.19 V and 0.27 V vs. Ag/AgCl for the samples with 0, 7 % at. C and 11 at. % C respectively. These values are close to the values in H_2SO_4 under OCP, which means that the involved redox reactions on the electrodes' surface take place at the same potential in both electrolytes. Nyquist (Fig. 4c) and Bode plots (Fig. 4d) have been recorded at 0.20V, 0.22V and 0.26V vs. Ag/AgCl for the samples with 0, ~7 at. % C and ~11 at. % C respectively in HCl, corresponding to their OCP values after 45min immersion in the electrolyte. In the Nyquist

diagram, the plots tend to be as a straight line close to the imaginary axis, indicating a ''capacitive'' behavior and corrosion resistant coatings under OCP conditions, very similar to H_2SO_4. In the phase Bode plot, the phase angle is between 84.0° to 85.3° degrees at the lowest frequency value (100 mHz). The results confirm that the films are corrosion resistant in HCl under OCP conditions. After that, the potential was scanned from –0.7 to 1.5 V vs. Ag/AgCl in HCl with a scan rate of 1mV/sec (Fig. 4b). The E_{corr} is slightly shifted to more noble values for the carbon contained films i.e. -0.39V vs Ag/AgCl for the carbon-free sample, -0.37 V and -0.34 V vs Ag/AgCl for the ~7 at. % C and ~11 at. % C respectively. The j_{corr} values are about 7.7×10^{-6} A/cm^2 for the carbon-free film, 7.1×10^{-6} A/cm^2 and 4.3×10^{-6} A/cm^2 for the ~7 at. % C and ~11 at. % C respectively. Similar to H_2SO_4, in HCl the transpassive region starts at about 0.85 V vs Ag/AgCl for all samples. Significant changes on the shape of the polarization curves are observed above 0.85 V vs Ag/AgCl. The carbon contained samples, show two current peaks at 1.1V vs Ag/AgCl and at 1.4V vs Ag/AgCl, with significant drop at about 1.2V vs Ag/AgCl, while a current increase, followed by a current drop was observed for the carbon free sample.

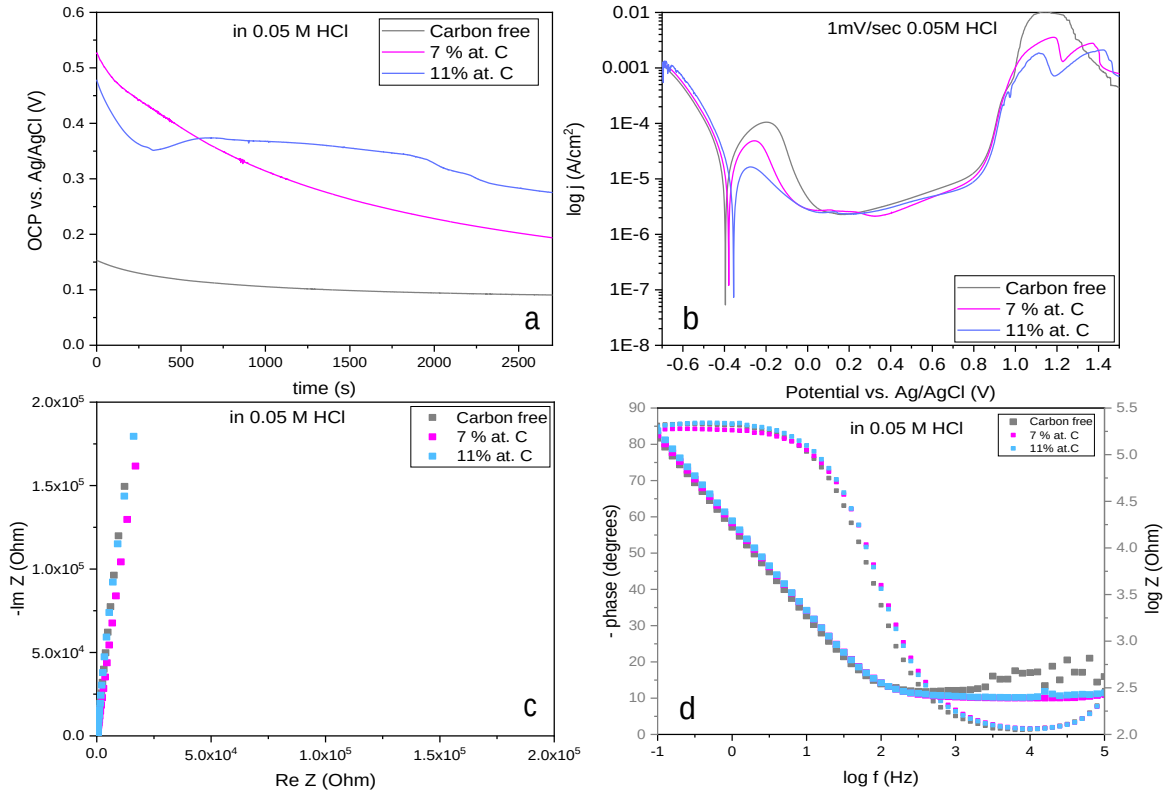

Figure 4: Electrochemical experiments in 0.05 M HCl: (a) Open circuit potential (OCP) vs. time plot, (b) polarization curves from -0.7 V to 1.5 V vs Ag/AgCl with a scan rate of 1 mV/s (c) Nyquist and (d) Bode plots obtained after 45 minutes at the OCP.

Short discussion on the electrochemical results: The electrochemical results in both electrolytes showed that the addition of carbon changed the shape of the polarization curves.

For potentials between -0.7 V and 0.85 V vs. Ag/AgCl (3 M NaCl):

- No significant differences in the cathodic part of the polarization curves in both electrolytes.
- No significant differences were observed between the two different electrolytes, but only among the carbon free and carbon contating samples.
- The results showed a difference in the oxidation charge in the passive region, which is associated with the dissolution and formation of the passive layer. The charge values are lower for a higher carbon content in the films, which indicates that for more carbon in the coating, less metal would need to be oxidised in order to obtain a passive film. This indicates that carbon would serve as an additional passive element.

An initial hypothesis suggested by Zendejas Medina et al. [6] was that carbon enrichement could exist underneath the oxide layer, acting as a blocking element for a further dissolution of the metals. To futher explore this hypothesis a ~7 at.% C was scanned from -0.7 V to 0.25 V vs Ag/AgCl in 0.05 M H_2SO_4, and then an XPS sputter depth profile with 200 eV Ar^+ ions for 1, 3, 5, 7, and 10 min was performed. From the results, which can be seen in Figures 5a and 5b for carbon C1s and O1s respectively, it could be concluded that after a minute of sputtering, a single contribution to the C1s peak was found at 283.2 eV which is the reported for carbon-metal (C-Me) binding energies [6,16]. This indicated that the carbon was fully incorporated into the alloy. The intensity of the peak increased with the sputtering time until it stabilized after five minutes. The lower C1s signal closer to the surface indicated that the carbon content in the oxide layer was lower than in the bulk of the film but a carbon enrichment (as suggested in the previous work [6]) could not be detected underneath the oxide layer.

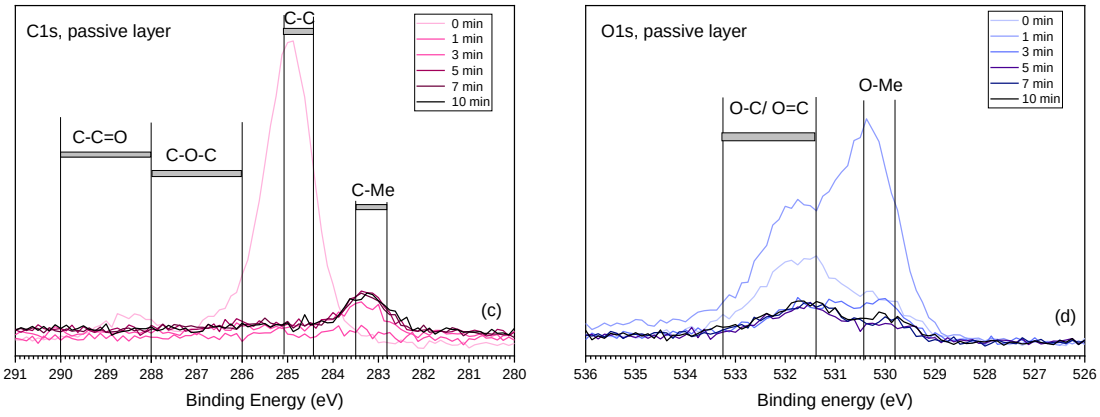

Figure 5: Sputter depth profile performed with XPS on a sample with 7 at. % C for (a) the C1s core level (b) the O1s core level and after a polarization curve in 0.05 M H_2SO_4 scanning from -0.7 V to 0.25 V vs Ag/AgCl. The different curves correspond to different sputter times, from 0 to 10 minutes. Binding energy intervals from the literature are included for C1s [11] and O1s [12] in various organic compounds, C1s in transition metal-carbon films [13,14], O1s in the oxides of Cr, Mn Fe, Co, and Ni [15].

Based on the calculations of the oxidation charges and the XPS depth profile (Figure 5) it is reasonable to assume that an increased carbon concentration in the coatings may lead to a blocking of the sites needed for the diffusion of the metals, required for their oxidation and subsequent dissolution in the electrolyte. The presence of a carbon enriched layer underneath the oxide layer [26] could, however, not be verified.

For potentials between -0.7 V and 1.5 V vs. Ag/AgCl:

After the end of the polarization curves the carbon free and the carbon containing samples were tested by XPS means (Figure 6). The use of the 3p region was important to avoid any Auger peak overlapping (Figure 6a) [10]. The XPS results showed that:

- *The surface of a carbon free sample after a polarization curve in 0.05 M H_2SO_4 was Mn-rich (Figure 6b):*

A possible explanation: The MnO_2 formation, should thermodynamically be possible prior to the oxidation of Cr_2O_3 to Cr(VI) :

$MnO_2 + 2e^- + 4\ H^+ \leftrightarrow Mn^{2+} + 2\ H_2O$, E^0 =1.02 V vs. Ag/AgCl (3 M NaCl)

$2\ HCrO_4^- + 6\ e^- + 8\ H^+ \leftrightarrow Cr_2O_3 + 5\ H_2O$, E^0 =1.15 V vs. Ag/AgCl (3 M NaCl)

If the MnO_2 starts forming prior to the formation of Cr(VI), then the MnO_2 could protect the Cr_2O_3 and all the other elements such as Co, Fe, and Ni present under the Cr_2O_3 passive layer, increasing the corrosion resistance above 0.85 V vs Ag/AgCl (3 M NaCl).

- *The surface of a carbon free sample after a polarization curve in 0.05 M HCl was fully etched away.*

  A possible explanation: The MnO_2 layer was not formed in this electrolyte, and the etching process was fast due to the formation of Cr(VI) along with the dissolution of Mn, Co, Fe, and Ni

- *The surface of a carbon contained sample after a polarization curve in 0.05 M H_2SO_4 was Cr-rich (Figure 6b):*

A possible explanation: The MnO_2 formation, should thermodynamically be possible prior to the oxidation of Cr_2O_3 to Cr(VI):

$MnO_2 + 2e^- + 4\ H^+ \leftrightarrow Mn^{2+} + 2\ H_2O$, E^0 =1.0 V vs. Ag/AgCl (3 M NaCl)

$2HCrO_4^- + 6\ e^- + 8\ H^+ \leftrightarrow Cr_2O_3 + 5\ H_2O$, E^0 =1.15 V vs. Ag/AgCl (3 M NaCl)

$C + 2\ H_2O \leftrightarrow CO_2 + 4\ H^+ + 4\ e^-$, E^0 = 0.02 V vs. Ag/AgCl (3 M NaCl)

$C + 2\ H_2O \leftrightarrow CO + 2\ H^+ + 2\ e^-$, E^0 = 0.31 V vs. Ag/AgCl (3 M NaCl)

In H_2SO_4 the etching process for carbon is observed above 0.4 V vs. Ag/AgCl (3 M NaCl) (results are not given in this report). The high currents seen for the carbon-containing samples should involve multiple reactions such as the oxidation of Cr(III) to soluble Cr(VI), the production of CO and/or CO_2 along with the oxidation and subsequent dissolution of the other metals.

- *The surface of a carbon contained sample after a polarization curve in 0.05 M HCl was Mn-rich*

A possible explanation: The MnO_2 formation, should thermodynamically be possible prior to the oxidation of Cr_2O_3 to Cr(VI)

$MnO_2 + 2e^- + 4\ H^+ \leftrightarrow Mn^{2+} + 2\ H_2O$, E^0 =1.02 V vs. Ag/AgCl (3 M NaCl)

$2\ HCrO_4^- + 6\ e^- + 8\ H^+ \leftrightarrow Cr_2O_3 + 5\ H_2O$, E^0 =1.15 V vs. Ag/AgCl (3 M NaCl)

$C + 2\ H_2O \leftrightarrow CO_2 + 4\ H^+ + 4\ e^-$, E^0 = 0.02 V vs. Ag/AgCl (3 M NaCl)

$C + 2\ H_2O \leftrightarrow CO + 2\ H^+ + 2\ e^-$, E^0 = 0.31 V vs. Ag/AgCl (3 M NaCl)

In HCl the formation of CO and/or CO_2 interacts with the chlorine evolution reaction: $2\ Cl^- + 2\ e^- \leftrightarrow Cl_2$, E^0 =1.16 V vs. Ag/AgCl (3 M NaCl)

According to Entwisle [17] under Cl_2 production, the production of CO and CO_2 which consume graphite are inhibited reactions, controlling the consumption or corrosion of the graphite. In this case a higher corrosion resistance is observed very likely due to a less pronounced oxidation of carbon along with the formation of a Mn-rich oxide layer on the films surface.

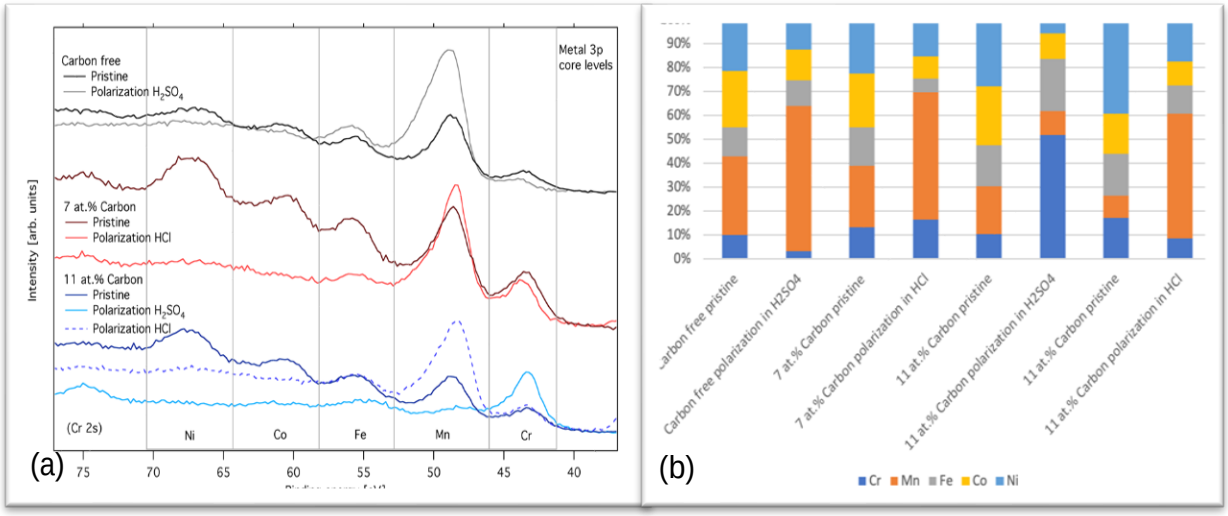

Figure 6: XPS metal 3p region for the pristine carbon free (black) thin film and after the recording of a polarization curve up to 1.5 V vs. Ag/AgCl (3 M NaCl) in 0.05 M H_2SO_4 (grey line). The pristine 7 at.% carbon-containing sample (wine red line) and after a polarization curve up to 1.5 V vs. Ag/AgCl (3M NaCl) in 0.05 M HCl (red line). The pristine ~11 at.% carbon-containing sample (dark blue line), after a polarization curve up to 1.4 V vs. Ag/AgCl (3 M NaCl) in 0.05 M H_2SO_4 (light blue line) and after a polarization curve in up to 1.5 V vs.

Ag/AgCl (3 M NaCl) 0.05 M HCl (blue dotted line) (a). Relative intensities of the different elements obtained by fitting the metal 3p core levels (b). For each element, the sums of the metallic and oxidation components are shown.

The SEM results for the 11 at.% C samples showed that the surface of the coatings was more porous after the polarization curve experiments in 0.05 M H_2SO_4 (Figure 7 left) than in 0.05 M HCl (Figure right). This is related to the fact that the corrosion resistance is higher in HCl than in H_2SO_4. The results are in accordance with the lower current values in HCl for the carbon contacting samples in the polarization curves (Figure 4b).

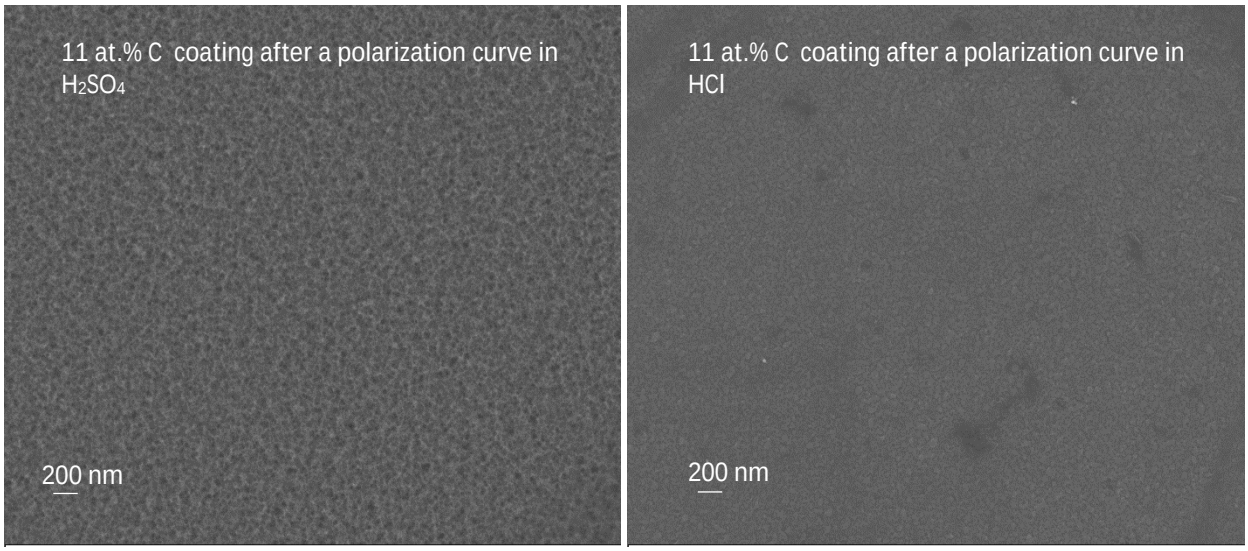

Figure 7: Top view of the SEM images of the 11 at.% carbon containing samples, after a polarization curve in 0.05 M H2SO4 (left) and in 0.05 M HCl (right).

Conclusions

The carbon presence and its effect on the corrosion resistance of near-equimolar CoCrFeMnNi magnetron sputtered films has been investigated in 0.05 M H_2SO_4 and 0.05 M HCl. The addition of carbon to the films was found to alter the morphologies, structures and corrosion resistances of the films. Dense and amorphous films were seen with the addition of small amount of carbon (~7 at. % C). The results indicate that the corrosion resistances depend on the type of used electrolyte (i.e., 0.05 M H_2SO_4 or 0.05 M HCl) and show the beneficial role of carbon regarding the corrosion resistance in the presence of Cl^- ions. Due to a less pronounced oxidation of carbon

and the formation of a Mn-rich oxide layer, the carbon-containing samples showed a higher corrosion resistance at high potentials (i.e., above 1.0 V vs. Ag/AgCl (3 M NaCl)) in HCl. The results of this study are promising for the design of new lightweight materials with compositions similar to those of stainless steels and highly improved corrosion resistances in Cl^- containing media.

Participation to conferences and papers

Results performed within this project, were presented as following:

- Poster submission (71st Annual Meeting of the International Society of Electrochemistry (Online event)
- Oral presentation (Inorganic days, webinar, November 19th 2020)
- A paper including the results of this work has been submitted to *Electrochimica Acta* magazine on Oct 21th 2021, with the title: ''Corrosion studies on multicomponent CoCrFeMnNi(C) thin films in acidic environments'' Eirini-Maria Paschalidou, Rebecka Lindblad, Leon Zendejas Medina, Dennis Karlsson, Ulf Jansson, Leif Nyholm (under review)

Acknowledgements

E.M. Paschalidou is grateful to ÅForsk for financially supporting Uppsala University for this project. This study was also supported by FunMat-II project that is financially supported by Vinnova (grant no 2016-05156). Rebecka Lindblad, Leon Zendejas Medina, Dennis Karlsson, Ulf Jansson, Leif Nyholm are also thanked for their assistance to this project.

Financial reporting

The following page gives an overview of the financial status of the project. Unfortunately, no trips could be made to attend conferences due to the COVID-19 pandemic, but only web conference participation was possible. Hence, a larger proportion of the costs were made towards salary.

Projekt 139604901

Agreement: 20-310

Huvudprojektledare: Eirini-Maria Paschalidou

Bidragsintäkter	472,000.00
Summa intäkter	472,000.00
Projektledarens lönekostnader	-339,235.67
Lönekostnader forskare	
Lönekostnader postdoktorer	
Lönekostnader forskarstuderande	
Lönekostnader andra	
Utrustning /Avskrivning	
Material	
Resor	-773.29
Administration	
Information	
Konsulter	
Övriga kostnader	
Summa kostnader	-340,008.96
Universitetets OH	-156,991.04
Summa kostnader inkl påslag	-497,000.00
Utfall	-25,000.00
Kvarstående utbetalning efter redovisning	25,000.00
Slutligt utfall	0.00

References

1. J. Wang et al. / Engineering 4 (2018) 352–360
2. J.-H. Wee / Renewable and Sustainable Energy Reviews 14 (2010) 735–744
3. L.E. Klebanoff et al. / Transportation Research Part D 54 (2017) 250–268
4. Cantor, B. et al. / Mater. Sci. Eng. A 375 (2004) 213–218
5. Gludovatz, B. et al. / Science 345 (2014) 1153–1158
6. L. Z. Medina et al. / Materials & Design 205 (2021) 109711
7. A. Hermann et al./ International Journal of Hydrogen Energy 30 (2005) 1297-130
8. A. Atrens et al. / *J. Electrochem. Soc.* 144 (1997) (11) 3697-3704.
9. I. Betova et al. /Corr. Sci. 44 (2002) 2675-2697
10. L. Wang et al. /Corros. Sci. 167 (2020) 108507.
11. J.F. Moulder, W.F. Stickle, P.E. Sobol, K.D. Bomben, Handbook of X-ray photoelectron spectroscopy
12. G. Beamson, D. Briggs, High Resolution XPS of Organic Polymers: The Scienta ESCA300 Database, 1992
13. T. Suszko et al. /Scr. Mater. 136 (2017) 24–28
14. K. Nygren, et al. Appl. Surf. Sci. 305 (2014) 143–153.
15. M.C. Biesinger et al. / Appl. Surf. Sci. 257 (2011) 2717–2730
16. T. Suszko et al. / Scr. Mater. 136 (2017) 24–28.
17. J.H. Entwisle et al. / J. Appl. Electrochem 4 (1974)